# STATIC AND DYNAMIC FRACTURE MICROMECHANICS OF SINTERED STEELS: A REVIEW

**M. Kabátová, E. Dudrová, A. S. Wronski**

***Abstract***

*In sintered steels there is evidence for static, as well as dynamic, loading that microcracks are nucleated, grow and coalesce, before attaining catastrophic size (Stage III in fatigue) for which fracture mechanics holds. The mechanisms are step-wise, thus Paris type analysis, applied e.g. to artificial cracks, does not apply. These processes were studied by combining fractography with surface replication of the most highly stressed region of specimens undergoing three-point bending, as progressively the tensile stress or the number of fatigue cycles was increased. Typically 10-20 microcracks were nucleated, some were arrested, others grew and coalesced until the final coalescence resulted in the catastrophic crack. Assuming semi-elliptical shape for the surface microcracks, the local stress intensity factor, $K_a$ was calculated for each microcrack using Irwin's formula. Initial values of $K_a$ were 1-4 MPa.m$^{1/2}$ and the eventual values correspond well to $K_{1C}$, independently determined.*

***Keywords: fracture mechanics, fracture micromechanics, sintered steels, microcrack growth, microcrack coalescence, catastrophic crack propagation.***

## INTRODUCTION

Failure of sintered steels, in static and dynamic loading, has been extensively investigated, especially by fractography and fracture mechanics techniques, e.g. Refs. [1,2] and Table 1. Special attention has been paid to (micro)crack nucleation and crack propagation, and their associations with porosity and resultant stress concentrations [3], generally neglecting the important stage of microcrack growth and coalescence [2,4]. Literature data exist on the roles of (especially interconnected) porosity [5,6], the surface [5-7] and prior particle boundaries [8,9] in the failure mechanisms. Polasik et al. [5,8] used a surface replication method to examine fatigue initiation and growth of microcracks in binder-treated Fe-0.85/0.5Mo-1.5Cu-1.75Ni-0.6C. They reported subcritical crack growth and deflection, leading to a tortuous path on the specimen surface ('*c*' dimension of the crack), estimated $\Delta K$ and constructed d$a$/d$N$–$\Delta K$ plots up to $\Delta K$ of 10 MPa m$^{1/2}$. Piotrowski et al. [10], however, concluded earlier that the contribution to fatigue resistance from crack deflection is small and reported that in coarse pearlite the speed is three times lower than that in Ni-rich regions of PM Fe-0.85Mo-2Ni-0.6C.

Detailed qualitative fatigue crack path studies were made by Bergmark et al, eg. Ref. 11., by successive surface grinding in steps of about 20 μm, and recording the surface crack in each level by light microscopy. Examination of e.g. fatigued Ni–Cu-Mo PM steel showed that crack paths went through high temperature bainite or along the interface

Margita Kabátová, Eva Dudrová, Institute of Materials Research of SAS, Watsonova 47, 040 01 Košice, Slovakia
Andrew S. Wronski, AGH University of Science and Technology, Al. Mickiewicza 30, 30-059 Kraków, Poland

between martensite and high temperature bainite. Ni-rich austenite was surrounded by martensite, which hindered the crack from entering into austenite. This indicated that austenite as such was not a strong crack stopper.

Failure initiation in static loading has been investigated in detail by Dudrova and Kabatova [1] and in Fe-Ni-Cu-Mo-C alloys crack nucleation stresses were found to be lower than the yield stress, typically $0.2\text{-}0.4\sigma_Y$, as in sintered high-speed steels [12]. Favoured nucleation sites included weak [contaminated] interfaces, especially prior particle boundaries, inclusions, pores and their agglomerates [1-4, 7]. These freshly-nucleated microcracks have irregular contours, cannot be easily modelled and are quite unlike the cleavage cracks postulated to form by dislocation interactions. Their sizes range from 5 to 20 microns.

Tab.1. Metallographic and theoretical [LEFMs] data for critical crack size.

| Material | $\sigma_y$ [MPa] | $\sigma$ [MPa] | $K_{IC}$ [MPa.m$^{1/2}$] | $\psi$ | $a_{crit}$ calculated [μm] | $a_{crit}$ measured [μm] |
|---|---|---|---|---|---|---|
| DistAE+0.7C | 466 | 603 | 25 | 0.71 | 390 | 350 - 420 |
| CrL+0.3C | 442 | 588 | 28 | 0.69 | 502 | 400 - 550 |
| CrL+0.7C cooled at 10$^0$C/min | 510 | 652 | 25 | 0.72 | 337 | 200 -300 |
| CrL+0.7C cooled at 50$^0$C/min | 617 | 806 | 36 | 0.71 | 449 | 400-500 |
| Fe-3Cu-0.7C | 340 | 530 | 28 | 0.58 | 514 | 480 - 550 |

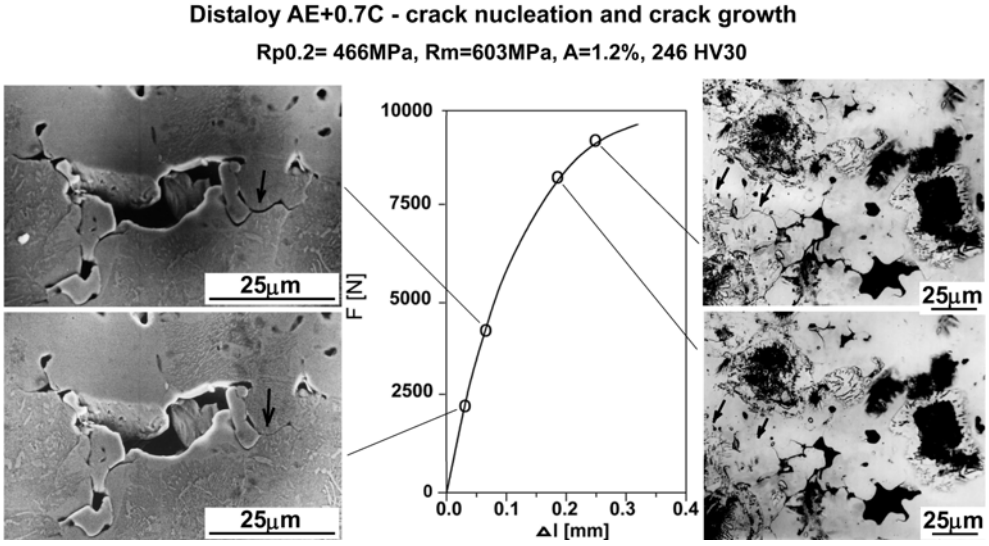


Fig.1. Microcrack nucleation and growth in Fe-4 Ni-1.5 Cu-0.5 Mo-0.7C 0.7C.

Very recently Torralba et al [3] examined tensile failure in three steels: ferritic–pearlitic Fe–C, bainitic prealloyed Fe–Mo–C and diffusion alloyed Fe–Ni–Cu–Mo–C through the combination of three techniques: plane stress tensile testing in the SEM, digital image correlation technique to trace the progress of local strain distributions during loading and fractography. They concluded that in all these steels cracks are generated during plastic

deformation and once cracks are generated, fracture progresses in a very fast mode. In situ observations on the tensile fracture mechanism in Fe-4Ni-1.5Cu-0.5Mo-0.5C have been also reported earlier by Wu et al [13]. In one specimen crack nucleation was detected at about half the UTS and no crack-initiation sites or propagation paths were identified on the other three specimens, because the fracture was fast and was completed before the stress was increased to the next level. They reported that the soft Ni-rich/C-lean areas around the pores were responsible for the failures.

Reference should be made to theoretical analyses and simulations [14-21] which consider that the final failure is preceded by coalescence of interacting microcracks which form a fatal crack that propagates unstably. Statistical models, based on probability theory, have been developed for evolutionary damage associated with nucleation, growth and linking of microcracks [16,20]. Ma et al [19] have claimed, however, that these models cannot account for details of crack growth and reported a simulation of the failure process of brittle specimens containing numerous stochastically distributed microcracks. These statistical approaches, however, do not appear to be applicable to step-wise microcrack growth.

Dudrova and Kabatova [1] concluded that crack growth is controlled by the same microstructural criteria as crack nucleation. Paths chosen are “easy” and microcracks can be stopped by pores or interfaces, or deflected, such that the driving force diminishes and the microcrack becomes non-propagating or dormant. Microcraks were reported to grow to some 400 microns, so conventional fracture mechanics could be employed in the interpretation of crack propagation. For the preceding stage, a stress intensity factor analysis can be carried out if the shape and size of the arrested microcracks are known, fracture micromechanics. Cracks are generally nucleated at the surface and thus that parameter can be measured pre-failure, by surface replica microscopy of progressively tensile loaded or fatigued specimens. The microcracks tend to be semi-eliptical and the Irwin formula [20]:

$$K_1 = \sigma \left\{ \left[ \frac{\Phi^2 - 0.212 \left(\frac{\sigma}{\sigma_y}\right)^2}{1.2} \right] \pi a \right\}^{0.5}$$

where σ is the tensile stress, a is the crack depth a, where σ is the tensile stress, a is the crack depth and Φ a geometric factor, should apply. Details will now be presented of the static [23] and dynamic [24] deformation of Fe-1.5Cr-0.2Mo-0.7C sintered in 75% $N_2$-25% $H_2$ at 1120°C. Sintered density was ~7.15 g.cm$^{-3}$, porosity ~7% with open porosity ~5% and grain size of ~6 μm. The microstructure comprised predominantly fine pearlite with some proeutectoid ferrite and upper and lower bainite. Macroscopic properties were: $R_{p0.2}$ = 617 MPa, $R_m$ = 806 MPa, A = 2.3 %, TRS = 1397 MPa, $K_{1C}$ = 36.2 MPa.m$^{1/2}$, fatigue limit ~ 240 MPa. The results do not substantially differ from another data set for the same material with a different processing history [4].

## RESULTS AND DISCUSSIONS

### Static Loading in Three-Point Bending of Fe-1.5Cr-0.2Mo-0.7C Steel

The microcrack detection procedure was to deposit a plastic replica [4,23] on the tensile face in the area of the prospective maximum stress, remove the replica, load the specimen to ~ 30% of the fracture stress, unload, deposit and remove a new replica in the same region, and repeat the procedure at several higher loads until failure of the specimen. Before each replica deposition, the critically stressed region was also photographed. 4-6 replicas of the region on the tensile face where failure was surface-initiated were made. These replicas were carbon sputtered before examination by optical microscopy. The

failure-initiating region was identified by SEM fractography and related to the orthogonal tensile surface containing pre-failure microcracks.

For both parts of the broken specimen, the fracture line is illustrated in Fig.2 and the corresponding failure initiating site region in Fig.3. The estimated periphery of the critical crack is outlined in Fig.4. Two microcrack systems coalescing are shown in Fig.5 and these coalesced with a third to form the critical crack, are outlined in Fig.6. This crack is related to the fracture line and also to the surface microcrack recorded for the highest pre-failure tensile stress, shown in Fig.7 [d and e]. Fig.7[a] shows this region before the specimen was stressed and Fig.7[b], Fig.7[c] and Fig.7[d] after loading to 72%, 88% and 99.6% of the bend strength, TRS, of 1355 MPa, respectively. No microcracks were detected after loading to 32 and 48% TRS. Table 2 summarizes sizes and shapes [c and a axes] of the near-elliptical failure-initiating microcracks forming and coalescing as the tensile stress is raised from 64 to 99.6 % of the fracture strength in bending, TRS.

Replicas removed at successively lower stresses from several specimens illustrate microcrack-microstructure interactions (e.g. Fig.8), including microcrack coalescence, growth and initiation of new microcracks. Regions adjoining the fracture path contained non-propagating microcracks with features making microcracking difficult. First indications of minute microcrack initiation were found at ~64% TRS. The microcracks were generally near elliptical, c-a, in shape and, in the failure-initiating zone, even the shallow microcracks tended to become semicircular. 3 microcrack systems were observed in the region examined: the system 1 eventually comprised 13 microcracks and there were 4 each in systems 2 and 3 [Table 2]. In crack system 1, microcracks a+b+c+d+e joined up, also (f+g)+h, all to coalesce at 99.6%TRS with i+j+(k+l)+m. For crack 2, microcrack n coalesced with (o+p+r) and for crack 3 microcracks s,t,v and z coalesced. All three, initially independent, microcrack systems grew and finally coalesced (Figs.5 and 6).

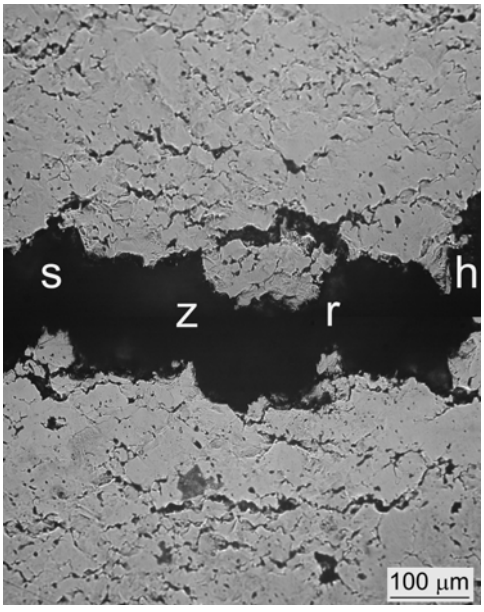


Fig.2.The fracture line on both parts of the broken specimen.

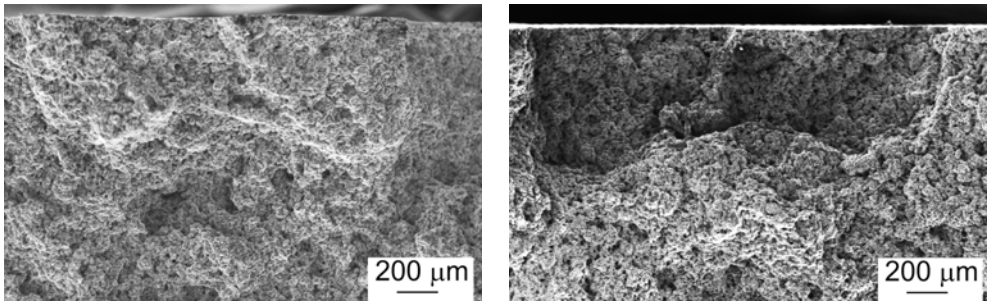


a) b)

Fig.3. Failure initiating site region on both parts of the broken specimen. Note the very irregular crack front periphery comprising coalesced microcrack systems.

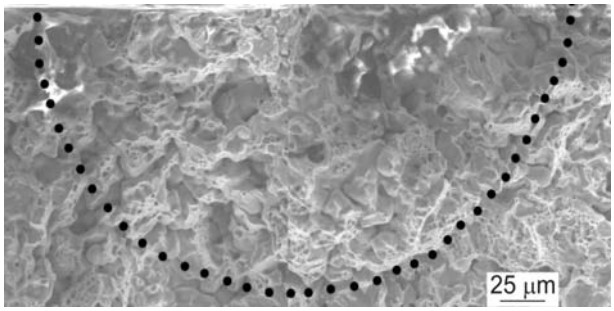


Fig.4. Fractographic identification of the critical crack with the microstructure dependent critical crack periphery outlined.

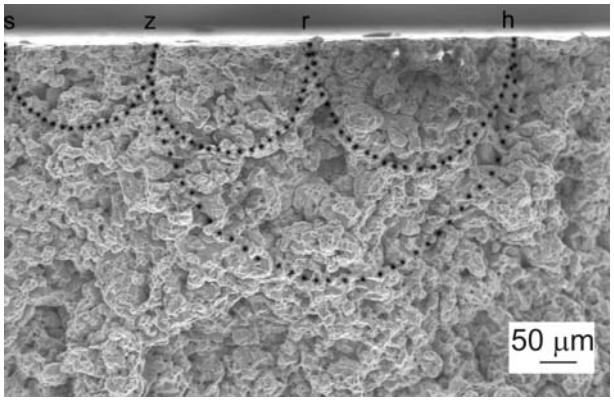


Fig.5. Coalescence of 2 outlined microcrack systems.

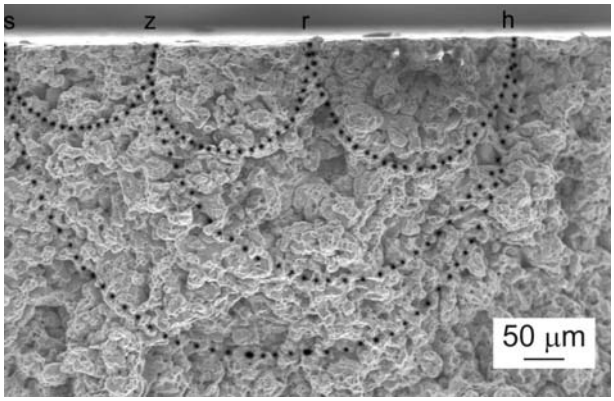


Fig.6. Coalescence of 3 microcrack systems preceding the formation of the catastrophic crack illustrated in Fig.4.

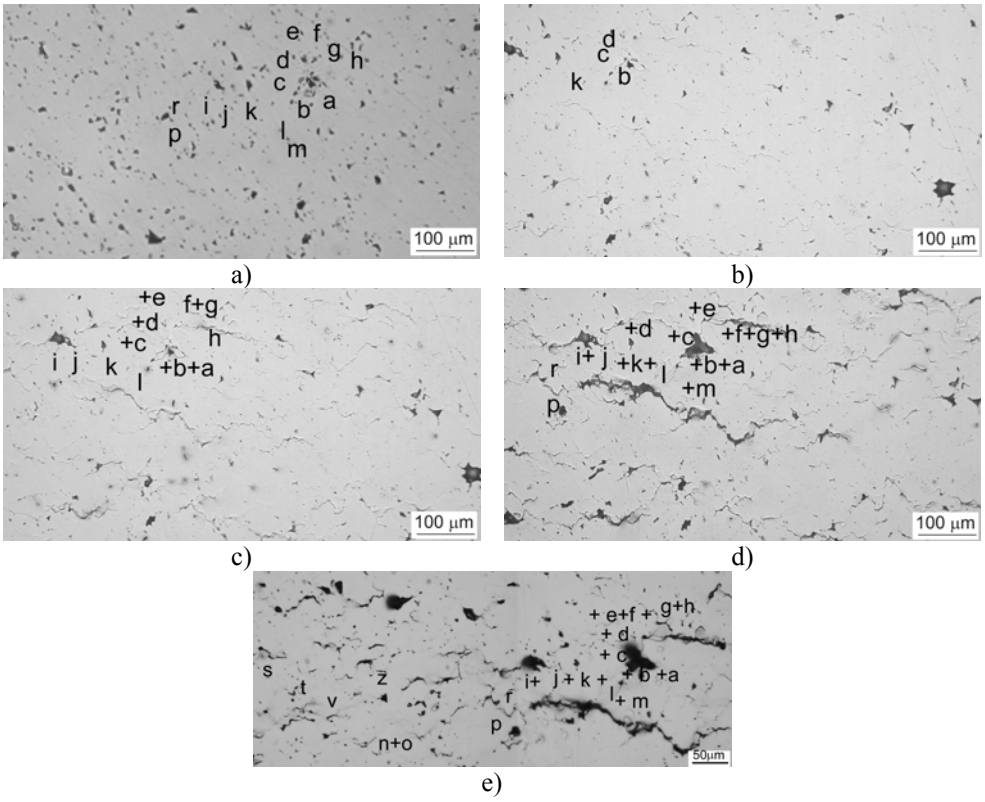


Fig.7. Replicas of the failure-initiating region on the tensile specimen surface, deposited before the specimen was loaded (a), and stressed to: 72% TRS (b), 88% TRS (c) and 99.6%TRS (d and e). Note in (b) initial microcracks b and c (generated at 64% TRS) and the new microcracks d and k, in (c) new, developing microcracks h, i, j and l and the initial coalescence (a+b+c+d+e) and (f+g), in (d) microcracks p and r and further coalescences of microcracks (a+b+c+d+e+f+g+h) and (i+j+k+l+m) and in (e) and (f) the 2 coalesced microcrack systems.

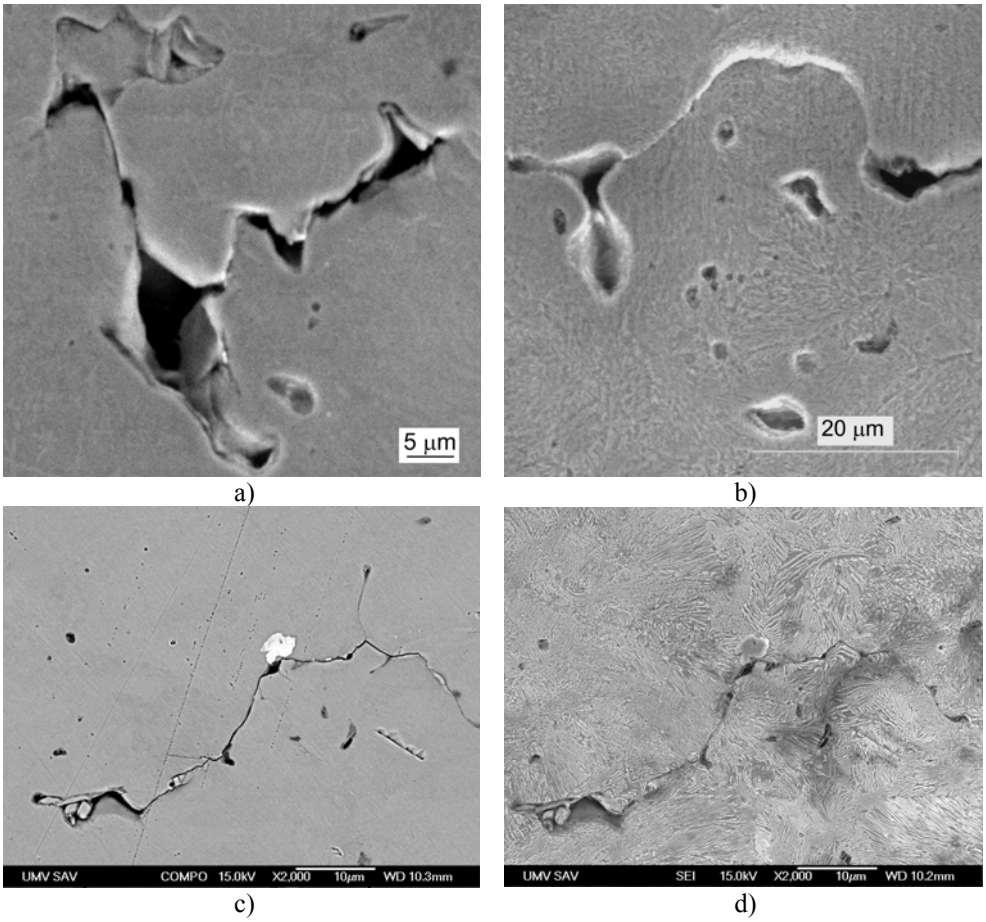


Fig.8. Examples of microcrack-microstructure interactions:(a) a pore stopping a microcrack growing along an interface, (b) a microcrack joining two pores, (c) polished surface, and (d) showing microstructure: a microcrack. following prior particle boundaries.

For each of the 21 microcracks the nominal stress intensity factor, $K_a$, was estimated using Irwin's [22] analysis for semi-elliptical cracks. The excellence of the agreement between $K_{1C}$ and the final $K_a$ in Table 2 [3 coalesced microcrack systems] is almost certainly fortuitous. For the single microcrack systems, the final $K_a$s were $< 0.6K_{1C}$. It should also be pointed out that, importantly, in this material, in contrast to high speed [12] and some structural PM steels [1], microcracking was only observed at stresses beyond the yield strength, as also by Torralba et al. [3] in their tensile testing experiments inside a scanning electron microscope.

Tab.2. Sizes and shapes [c and a axes, in μm] of the near-elliptical failure-initiating microcracks forming and coalescing as the tensile stress is raised from 64 to 99.6% of the transverse rupture strength, TRS. Note that no microcracks were detected when the specimen was stressed to 32 and 48% TRS. Also presented are estimates of the stress intensity factor $K_a$ [MPa.m$^{1/2}$]. When cracks 1 and 2 coalesced, $K_a \sim 0.7K_{1C}$, and failure took place at $\sim K_{1C}$ [independently estimated].

| Applied Load, σ [MPa] | | Crack 1 | | | | | | | | | | | | | Crack 2 | | | | Crack 3 | | | |
|---|---|---|---|---|---|---|---|---|---|---|---|---|---|---|---|---|---|---|---|---|---|---|
| | | a | b | c | d | e | f | g | h | I | j | k | l | m | n | o | p | r | s | t | v | z |
| 871 (64%) | *c* | | 4 | 5 | | | | | | | | | | | | | | | | | | |
| | *a* | | 3 | 4 | | | | | | | | | | | | | | | | | | |
| | $K_a$ | | **3.0** | **3.7** | | | | | | | | | | | | | | | | | | |
| 980 (72%) | *c* | | 4 | 5 | 0.8 | | | | | | | 6 | | | | | | | | | | |
| | *a* | | 4 | 5 | 0.5 | | | | | | | 4 | | | | | | | | | | |
| | $K_a$ | | **4.4** | **4.9** | **2.2** | | | | | | | **3.7** | | | | | | | | | | |
| 1089 (80%) | *c* | 3 | 13 | | 10 | 6 | 2 | 6 | | | | 6 | | | 1 | | | | | | | 3 |
| | *a* | 3 | 12 | | 8 | 4 | 2 | 6 | | | | 4 | | | 1 | | | | | | | 2 |
| | $K_a$ | **4.** | **7.9** | | **6.0** | **3.9** | **3.3** | **5.8** | | | | **3.9** | | | **2.4** | | | | | | | **2.8** |
| 1198 (88%) | *c* | | | | 38 | | 24 | | 7 | 5 | 3 | 6 | 19 | | 2 | | | | | | 5 | 3 |
| | *a* | | | | 28 | | 21 | | 5 | 3.5 | 2 | 4.5 | 13 | | 2 | | | | | | 5 | 3 |
| | $K_a$ | | | | **12.3** | | **10.7** | | **4.5** | **3.3** | **2.8** | **4.4** | **7.4** | | **3.5** | | | | | | **5.6** | **4.3** |
| 1307 (96.5%) | *c* | | | | | | 81 | | | 11 | 3 | 47 | | 6 | 7 | | 5 | 4 | 2 | 8 | 7 | 4 |
| | *a* | | | | | | 70 | | | 10 | 3 | 40 | | 5 | 6 | | 4 | 3 | 2 | 7 | 7 | 4 |
| | $K_a$ | | | | | | **20.1** | | | **7.8** | **4.5** | **16.1** | | **5.5** | **5.8** | | **4.6** | **2.4** | **3.7** | **6.4** | **6.9** | **5.2** |
| 1350 (99.6%) | *c* | | | | | | 82 | | | | | 75 | | | 9 | | 15 | 11 | 2 | 19 | 7 | 6 |
| | *a* | | | | | | 71 | | | | | 61 | | | 8 | | 14 | 10 | 2 | 19 | 7 | 5.5 |
| | $K_a$ | | | | | | **20.4** | | | | | **18.0** | | | **6.9** | | **9.4** | **7.0** | **3.7** | **11.5** | **7.0** | **5.6** |
| 1355 (100%) | *c* | | | | | | | | 212 | | | | | | 148 | | | | 119 | | | |
| | *a* | | | | | | | | 174 | | | | | | 135 | | | | 107 | | | |
| | $K_a$ | | | | | | | | **30.9** | | | | | | **29.1** | | | | **25.3** | | | |
| | *c* | | | | | | | | | | | 360 | | | | | | | 119 | | | |
| | *a* | | | | | | | | | | | 260 | | | | | | | 107 | | | |
| | $K_a$ | | | | | | | | | | | **34.2** | | | | | | | **25.3** | | | |
| | *c* | | | | | | | | | | | 479 | | | | | | | | | | |
| | *a* | | | | | | | | | | | 310 | | | | | | | | | | |
| | $K_a$ | | | | | | | | | | | **35.1** | | | | | | | | | | |

**Fatigue Loading of Fe-1.5Cr-0.2Mo-0.7C Steel**

The rectangular specimens 40x5x11 (reducing to 5 at centre) mm$^3$ were cyclically deformed in bending on a Schenck fatigue tester, operating at 24Hz with R = -1; the S-N curve is presented as Fig.9. The experimental procedure was as for the tensile specimens, except that the region of maximum stress for S = 312 MPa was now replicated before testing and after the test was stopped at these number of cycles, N, 100, 200, 400, 600, 700, 800, 1000, 2000, 3000, 4000, 5000, 6000, 7000, 8000, 9000, 10000, 11000, 12000, 15000, 18000, 21000, 23000, 25000, 27000, 30000, 33000, 36000, 39000, 42000 and 45000 cycles, with the specimen failing at N=49900. 4-6 replicas of the region where failure was expected to be initiated were made.

Using SEM fractography, the failure-initiating region was identified, always at the surface in these experiments, Fig.10.The same region (orthogonal to the fractograph) on both parts of the broken specimen was found, the fracture line photographed (Fig.11a) and the failure-originating site was then identified on the failure line and on the last pre-failure replica (Fig.11b). This same region was examined carefully on all the previously obtained

replicas - and photographed. Each microcrack was identified by a capital letter: A-S. The microcrack "2c"dimensions were transferred to the fractograph and thus, at each N, one dimension of each microcrack was known. Careful examination of the microfractographic features and, knowing that the microcrack shapes tend to be near elliptical, enabled sketching of the probable microstructure-determined microcrack fronts.

Microcracking was detected for some specimens examined after testing for only 100 cycles, e.g. Fig.12, crack D, indicating that analyses should consider microcrack initiation from the first cycle. At S = 312 MPa, within the first 700 cycles, further microcracks, B, C, E, K, O, P, R, S were nucleated and some grew, similarly for 700>N>3000, as illustrated in Fig.12. Microcrack nucleation continued with increasing N: F, H and J after 12000, and A at 15000 cycles. Continued growth of some cracks proceeded till 36000 cycles, illustrated in Fig.13, with the first coalescence of microcracks, E+F, occurring at 39000 cycles. Fresh microcracks were nucleated even in the last 10000 cycles: I, L, M, N, illustrated in Fig.14, but then coalescence became the predominant mechanism: A+(B+C+D)+(E+F)+(G+H)+I+J+K+L, t hen, + M+N+O + (P+R+S), giving the final non-propagating crack, Fig.11. The progressive growth of the very first detected microcrack D is shown in Fig.15. It is to be noted that, in this failure mechanism,18 microcracks were nucleated and (B+C+D), (E+F), (G+H) and (P+R+S) progressively joined before the final coalescence of the 2 systems A-L and P-S with M, N and O into the catastrophic crack.

Frequently non-propagating microcrack paths were mainly along prior particle boundaries, between the pores, but also transgranular and along and across cementite lamellae. To be noted are the observations of microcracks terminating, with local plastic flow at the crack tip, in the ferrite. Stage III failure was less transgranular and mainly by interparticle and ductile dimple modes.

The crack depths, "a" axes, were estimated when cycling was interrupted. Then all microcrack sizes (initial, extended and coalesced ), i.e. a and c values, were recorded, together with stress intensity factors, estimated using Irwin's formula [22] for $K_a$, throughout the fatigue life. Note that the initial $K_a$ values were as low as 1 MPa.$m^{1/2}$.

The calculations for the latter stages of the Stage II, 4200>N>4990, process, are presented in Fig.3. It is not possible to specify when exactly in the fatigue life microcrack growth, arrest and coalescence occurred, only record actual new crack size "2c" after the interval $\Delta N$ between successive observations. It is suggested that there was no progressive (classical), but only step-wise microcrack growth and coalescence. Such "staircase" growth is assumed in the schematics of Fig.16 illustrating the initiation and growth to 1000 cycles of the initial 8 microcracks, (a), further initiation and growth to 35000 cycles, (b), (c) and (d), and crack development between 35000 and 49900 cycles, i.e. up to the final joining of all the microracks into the Stage III fatigue crack. Accordingly it is impractical to plot $da/dN–\Delta K$ with any significance, noting that such plots are conventionally constructed for an artificial failure-originating crack.

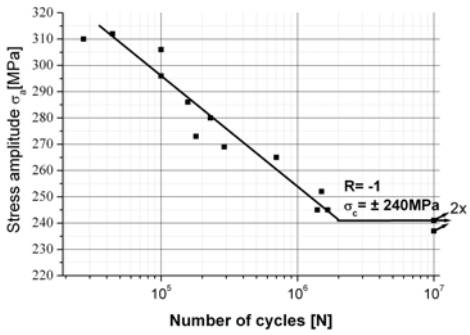


Fig.9. S-N curve for sintered Fe-1.5Cr-0.2Mo-0.7C steel.

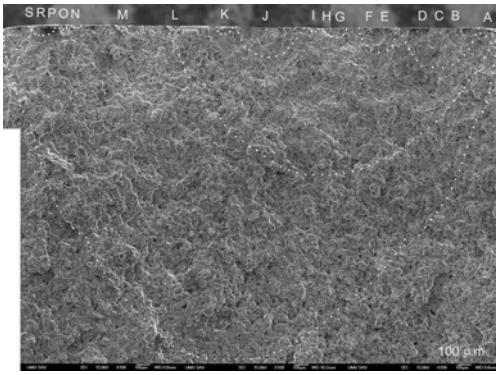


Fig.10. Collage of 12 micrographs of the failure originating area of the fracture surface. Outlined are the positions of the microcracks M, N and O and the crack systems P+R+S and A-L joining up to form the Stage III catastrophic crack.

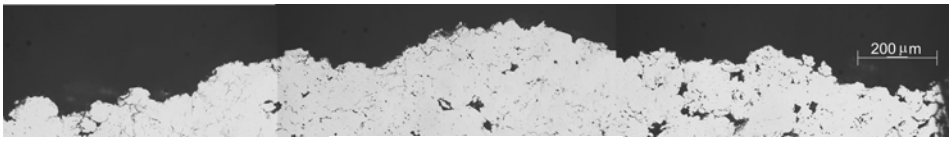


(a) Fracture line: c~2.4 mm

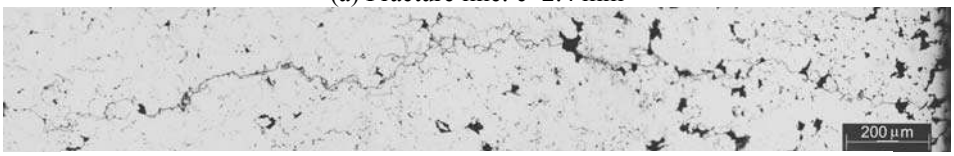


(b) Final pre-failure surface coalesced (micro)crack, 45000 cycles, c~ 1.5 mm

Fig.11. The fracture line and the matching failure-initiating microcrack system photographed after 4500 cycles.

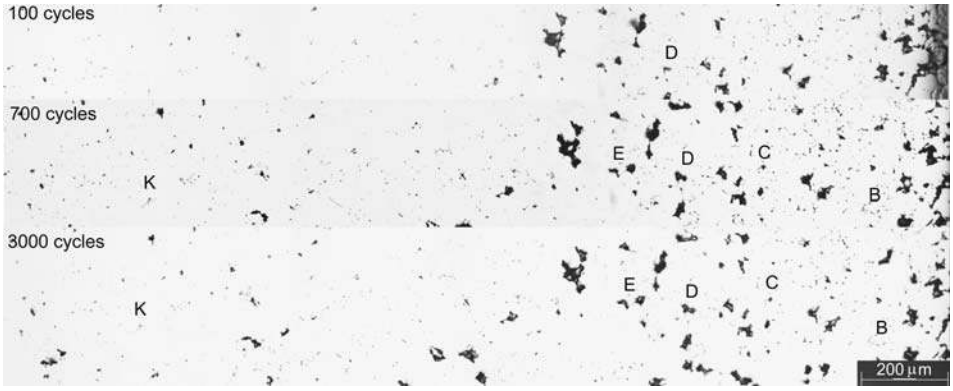


Fig.12. Microcrack initiation and development in the first 3000 cycles. Note that (i) microcrack D initiation within the first 100 cycles,(ii) at 700 cycles: growth of D and 4 new microcracks B, C, E nucleated at N=600 and K nucleated at N=200,(iii) growth of microcracks B, D, E and K between 700 and 3000 cycles, whilst C was dormant.

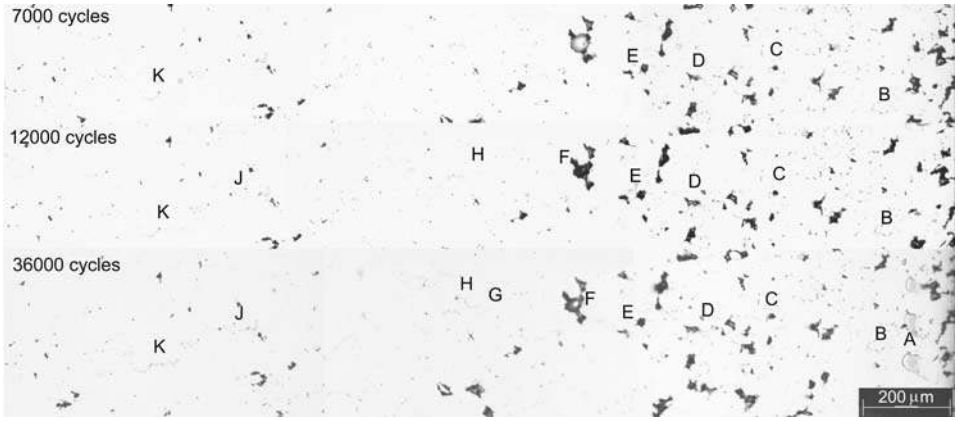


Fig.13. Microcrack development between 3000 and 36000 cycles. Note that: (i) of the 5 microcracks present at N=3000, only K grew to N=7000,between 7000 and 12000 cycles three new microcracks F, H, J were nucleated and that the preexisting microcracks B, C, D, E, and K all grew, (ii) between 12000 and 36000 cycles two new microcracks were nucleated, A at 15000 cycles, and G, and that the other microcracks B, C, D, E, F, H, J, K all grew.

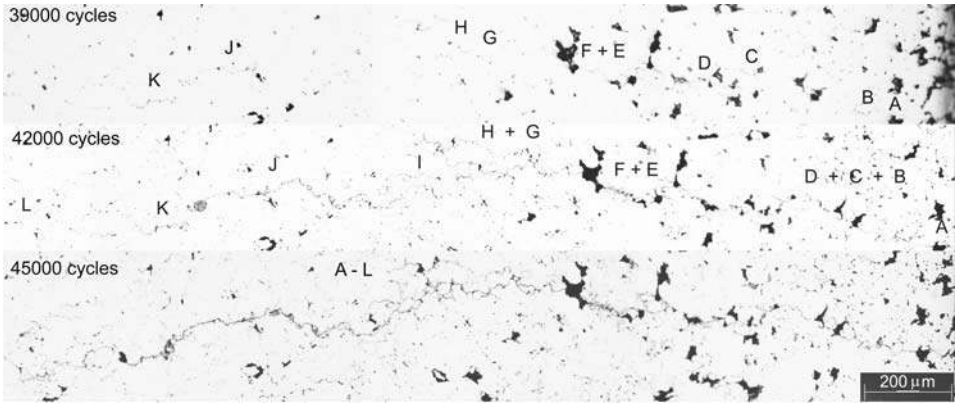


Fig.14. Microcrack development between 39000 and 45000 cycles. Note that: (i) microcracks A, D, G, J grew, E and F coalesced, while the others, B, C, H, K were all stopped, (ii) between 39000 and 42000 cycles nucleation of four new microcracks I, L, M, N, coalescence of B+C+D, G+H, P+R+S, and growth of the remaining microcracks A, J, K, (iii) between 42000 and 45000 cycles coalescence into c~1.5 mm microcrack of A+(B+C+D)+(E+F)+(G+H)+I+J+K+L.

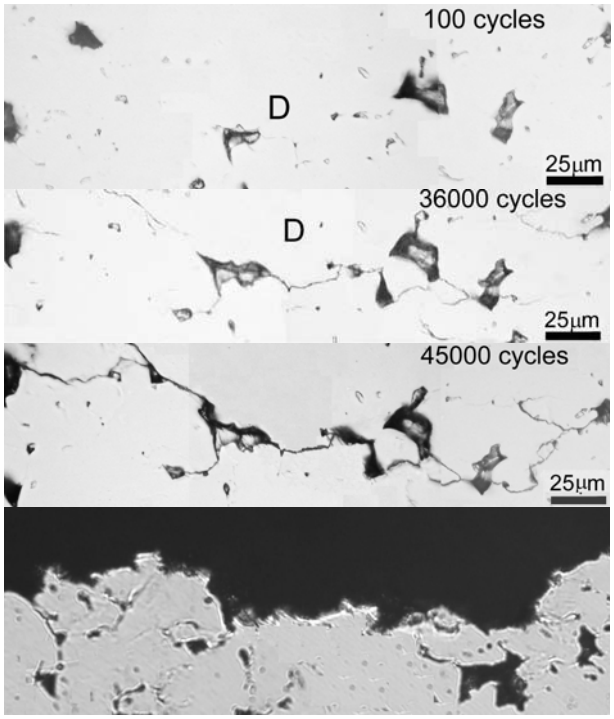


Fig.15. Detailed micrographs of the nucleation and growth of microcrack D detected within the first 100 cycles.

Tab.3. Sizes and shapes (c and a axes) of the near-elliptical microcracks I, L, M, N which finally nucleated, grew and coalesced with preexisting microcracks in the interval 42000-49900 cycles (failure). Values of N are generally upper bounds. Also presented are estimates of the stress intensity factor $K_a$.

| No of cycles N | Microcrack | A | B+C +D | E+F | G+H | I | J | K | L | M | N | O | P+R +S |
|---|---|---|---|---|---|---|---|---|---|---|---|---|---|
| 42000 | c μm | 90 | 363 | 224 | 127 | 37 | 299 | 63 | 30 | 37 | 30 | 60 | 96 |
| | a μm | 60 | 300 | 170 | 60 | 15 | 200 | 60 | 30 | 35 | 28 | 50 | 90 |
| | Φ | 1.32 | 1.44 | 1.39 | 1.19 | 1.15 | 1.32 | 1.53 | 1.57 | 1.53 | 1.51 | 1.44 | 1.52 |
| | **$K_a$, MPa.m** | **5.1** | **12.4** | **9.0** | **4.6** | **2.2** | **9.3** | **5.9** | **4.3** | **4.5** | **4.0** | **5.1** | **7.2** |
| 45000 | c μm | 1478 | | | | | | | | 37 | 30 | 60 | 96 |
| | a μm | 1000 | | | | | | | | 35 | 28 | 50 | 90 |
| | Φ | 1.33 | | | | | | | | 1.53 | 1.51 | 1.44 | 1.52 |
| | **$K_a$, MPa.m** | **20.9** | | | | | | | | **4.5** | **4.0** | **5.1** | **7.2** |
| 49900 | c, μm | 2390 | | | | | | | | | | | |
| | a, μm | 2250 | | | | | | | | | | | |
| | Φ | 1.52 | | | | | | | | | | | |
| | **$K_a$, MPa.m** | **36.0** | | | | | | | | | | | |

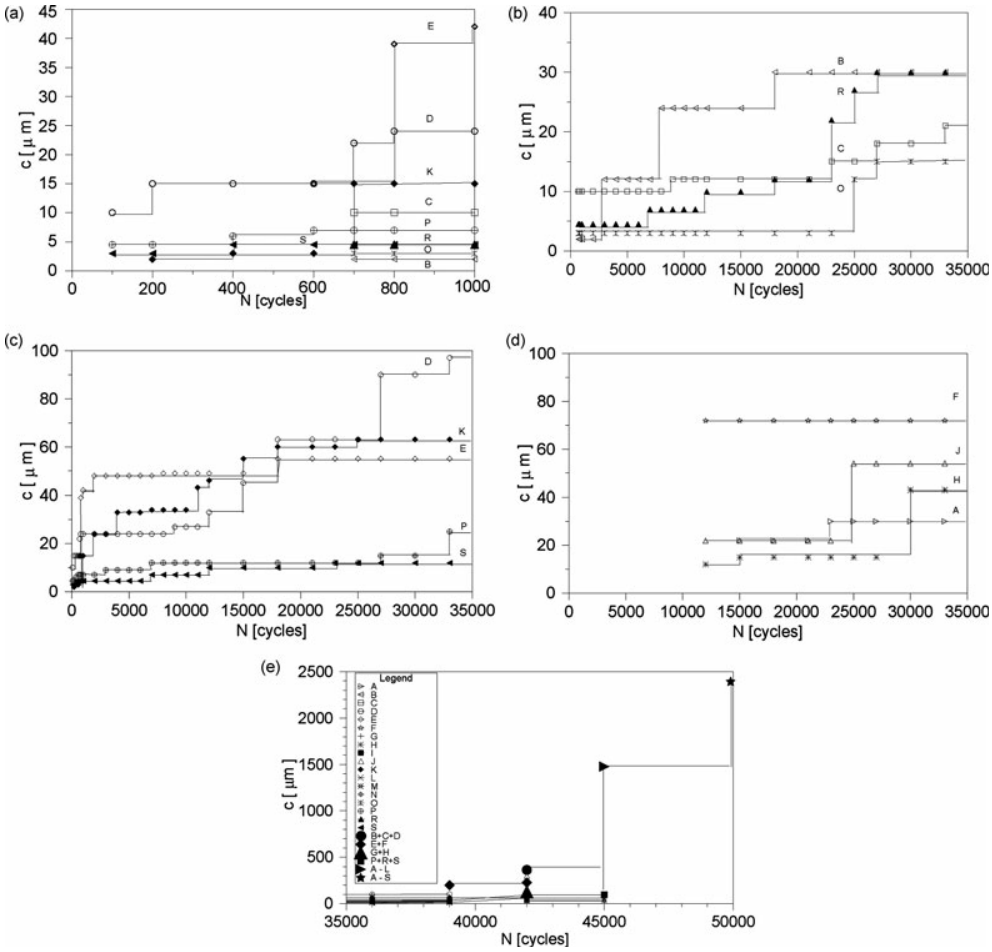


Fig.16. Schematics of microcrack initiation, growth and, coalescence- assuming 'stepwise' events: (a) to 1000 cycles of the initial nine microcracks: B, C, D, E, K, O, P, R, S, to 35 000 cycles of microcracks: (b) B, C, O, R, (c) D, E, K, P, S and (d) A, F, H, J, (e) between 35 000 and 49 900 cycles.

**Fatigue Loading of Fe-1.4Cr-0.2Mo-1.4Mn-0.7C Steel**

This steel was sintered in 90% $N_2$-10% $H_2$ at 1120°C to a density of 6.9 g $cm^{-3}$ [25]. The macroscopic properties were $R_{p0.2}$ = 498 MPa, $R_m$ = 548 MPa, A = 0.6 %, TRS = 905 MPa, $K_{1C}$ = 26 MPa.$m^{1/2}$, fatigue limit ~ 190 MPa (Fig.17). Similar observations, at R = 200 MPa, were carried out as for the Fe-1.5Cr-0.2Mo-0.7C steel; interestingly failure initiation took place at a specimen corner (Fig.18). Microcracking was detected after 100 cycles and a further 29 observations, were made before failure after 354300 cycles. Nucleation of 10 microcracks was detected, microcrack sizes ranged from <5 to ~20 µm and again there was stepwise microcrack growth and coalescence, up to critical crack 3.12 mm deep. $K_a$ ranged from 2-6 MPa.$m^{1/2}$ (fresh microcracks) to 27.3 MPa.$m^{1/2}$ in the material where independently determined $K_{1C}$ = 26 MPa.$m^{1/2}$.

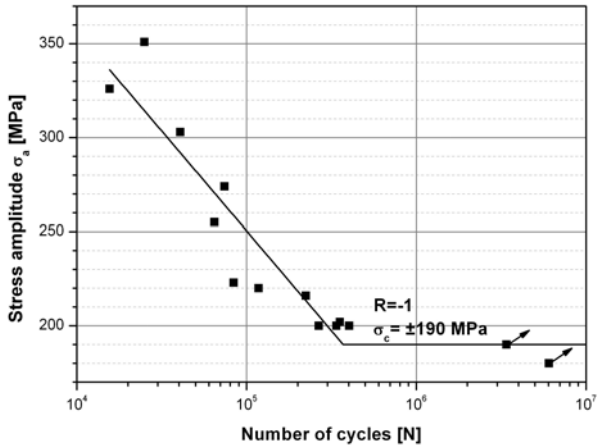


Fig.17. S-N curve for Fe-1.4Cr-0.2Mo-1.4Mn-0.7C steel.

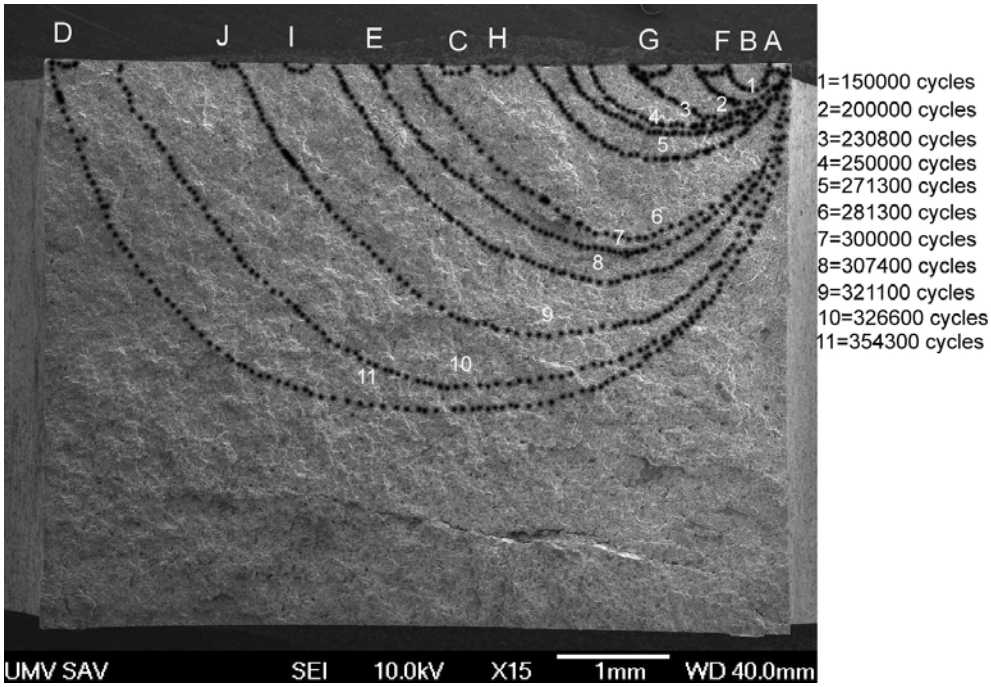


Fig.18. Fractograph of the fatigue failed Fe-1.4Cr-0.2Mo-1.4Mn-0.7C specimen, with positions of the crack front at various values of N indicated.

Details of the growth and coalescence of the microcracks, and the $K_a$ values are presented in Tables 4-6.

Tab.4. Microcrack sizes and stress intensity factors, $K_a$, for 100<N<130800 (only nucleation and growth).

| Number of cycles, N | Microcrack | A | B | F | C | E | D |
|---|---|---|---|---|---|---|---|
| 100 | c μm | 20 | | | | | |
| | a μm | 16 | | | | | |
| | **$K_a$ MPa.m$^{1/2}$** | **1.8** | | | | | |
| 3000 | c μm | 75 | | | | | |
| | a μm | 50 | | | | | |
| | **$K_a$ MPa.m$^{1/2}$** | **3.0** | | | | | |
| 10000 | c μm | 100 | | | | | |
| | a μm | 70 | | | | | |
| | **$K_a$ MPa.m$^{1/2}$** | **3.6** | | | | | |
| 50000 | c μm | 100 | 75 | | 25 | | 50 |
| | a μm | 70 | 50 | | 20 | | 46 |
| | **$K_a$ MPa.m$^{1/2}$** | **3.6** | **3.0** | | **2.0** | | **3.3** |
| 70000 | c μm | 135 | 100 | | 95 | 35 | 50 |
| | a μm | 100 | 70 | | 80 | 30 | 46 |
| | **$K_a$ MPa.m$^{1/2}$** | **4.4** | **3.6** | | **4.1** | **2.6** | **3.3** |
| 100000 | c μm | 135 | 165 | | 95 | 35 | 63 |
| | a μm | 100 | 120 | | 80 | 30 | 54 |
| | **$K_a$ MPa.m$^{1/2}$** | **4.39** | **4.7** | | **4.1** | **2.6** | **3.4** |
| 130800 | c μm | 135 | 215 | 50 | 95 | 35 | 63 |
| | a μm | 100 | 210 | 46 | 80 | 30 | 54 |
| | **$K_a$, MPa.m$^{1/2}$** | **4.4** | **7.2** | **3.3** | **4.1** | **2.6** | **3.4** |

Tab.5. Microcrack sizes and stress intensity factors, $K_a$, for 150000<N<281300.

| Number of cycles, A | Microcrack | A + B + F | G | H | C | E | D |
|---|---|---|---|---|---|---|---|
| 150000 | c μm | 500 | | | 95 | 35 | 63 |
| | a μm | 360 | | | 80 | 30 | 54 |
| | **$K_a$ MPa.m$^{1/2}$** | **8.21** | | | **4.1** | **2.6** | **3.4** |
| 200000 | c μm | 700 | 75 | | 95 | 35 | 63 |
| | a μm | 450 | 70 | | 80 | 30 | 54 |
| | **$K_a$ MPa.m$^{1/2}$** | **8.8** | **4.1** | | **4.1** | **2.6** | **3.4** |
| 230800 | c μm | 925 | | | 95 | 35 | 63 |
| | a μm | 550 | | | 80 | 30 | 54 |
| | **$K_a$ MPa.m$^{1/2}$** | **9.5** | | | **4.1** | **2.6** | **3.4** |
| 250000 | c μm | 1170 | | | 95 | 35 | 63 |
| | a μm | 600 | | | 80 | 30 | 54 |
| | **$K_a$ MPa.m$^{1/2}$** | **9.5** | | | **4.1** | **2.6** | **3.4** |
| 271300 | c μm | 1375 | | 150 | 100 | 35 | 63 |
| | a μm | 800 | | 120 | 96 | 30 | 54 |
| | **$K_a$ MPa.m$^{1/2}$** | **11.4** | | **4.95** | **4.8** | **2.6** | **3.4** |
| 281300 | c μm | 1560 | | | | 35 | 63 |
| | a μm | 1400 | | | | 30 | 54 |
| | **$K_a$ MPa.m$^{1/2}$** | **17.9** | | | | **2.6** | **3.4** |

Tab.6. Microcrack sizes and stress intensity factors, $K_a$, for 300000<N<354300 (ending with growth of the coalesced crack).

| Number of cycles, N | Microcrack | A + B + F + G + H + C + E | I | J | D |
|---|---|---|---|---|---|
| 300000 | c μm | 1930 | | | 63 |
| | a μm | 1600 | | | 54 |
| | **$K_a$ MPa.m$^{1/2}$** | **18.3** | | | **3.4** |
| 307400 | c μm | 1960 | 200 | | 63 |
| | a μm | 1920 | 160 | | 54 |
| | **$K_a$ MPa.m$^{1/2}$** | **22.0** | **5.7** | | **3.4** |
| 321100 | c μm | 2500 | | 165 | 63 |
| | a μm | 2400 | | 150 | 54 |
| | **$K_a$ MPa.m$^{1/2}$** | **24.2** | | **5.9** | **3.4** |
| 326600 | c μm | 3085 | | | 63 |
| | a μm | 2962 | | | 54 |
| | **$K_a$ MPa.m$^{1/2}$** | **26.9** | | | **3.4** |
| 354300 | c μm | 3300 | | | |
| | a μm | 3120 | | | |
| | **$K_a$ MPa.m$^{1/2}$** | **27.3** | | | |

The microcrack joining processes appeared easier through pores and interface areas, especially those contaminated - and this influences the deterioration in fatigue properties. Conversely, microcrack deflection and arrest were due to high-strength obstacles, specifically cementite lamellae in the fine pearlite, acting in a similar way e.g to the Ni-rich martensite regions in Fe-0.5/0.85Mo-1.5Cu-1.75Ni-0.6C [5, 8]. Another possible microcrack deflection/stopping mechanism could be the small grains produced by diffusion induced grain boundary migration (DIGM) around pores left by the diffused master alloy particles [26]. Again a Paris type analysis is not relevant to Stage II fatigue growth interpretation for this PM steel when fatigue is initiated by natural microcracks.

## CONCLUSIONS

- Static loading nucleates microcracks at defects, in some steels at stresses below the yield stress
- Fatigue loading can nucleate microcracks in the first 100 cycles giving
- $K_a < 2$ MPa.m$^{1/2}$
- Numerous microcracks are nucleated; they grow, some are arrested, some coalesce and eventually propagate
- Growth and coalescence are step-wise processes
- Properties of propagating microcracks, in static and dynamic loading, are those of conventional cracks
- Fracture micromechanics -> Fracture Mechanics.

**Acknowledgement**

The authors wish to thanks to the Slovak National Grant Agency (Project VEGA 2/0052/14, 2/0100/15) for financial supporting of this work.

## REFERENCES

[1] DUDROVÁ, E., KABÁTOVÁ, M. In: Proc.Euro PM 2004. Vol. 3. Eds. H. Danninger,

R. Ratzi. EPMA, 2004, p. 193
[2] KABÁTOVÁ, M., DUDROVÁ, E., HRUBOVČÁKOVÁ, M. In: Proc.Euro PM 2011. Vol. 1. EPMA, 2011, p. 39
[3] TORRALBA, JM., ESTEBAN, L., BERNARDO, E., CAMPOS, M.: Powder Met., vol. 57, 2014, p. 357
[4] KABÁTOVÁ, M., DUDROVÁ, E., WRONSKI, AS.: Powder Met. Progr., vol. 5, 2005, p. 185
[5] POLASIK, SJ., WILLIAMS, JJ., CHAWLA, N.: Metall. Mater. Trans. A, vol. 33A**,** 2002, p. 73
[6] CHRISTIAN, KD., GERMAN, RM.: Int. J. Powder Metall., vol. 31**,** 1995**,** p**.** 51
[7] DANNINGER, H., SPOLJARIC, D., WEISS, B.: Int. J. Powder Metall., vol. 33, 1997, p. 43
[8] CHAWLA, N., POLASIK, S., NARASIMHAN, KS., MURPHY, T., KOOPMAN, M., CHAWLA, KK.: Int. J. Powder Metall., vol. 37, 2001, p. 49
[9] HADRBOLETZ, A., WEISS, B.: Int. L Mater. Rev., vol. 42**,** 1997, p. 1
[10] PIOTROWSKI, G., DENG, X., CHAWLA, N.: Fatigue Fract Engng Mater Struct., vol. 32, 2004, p. 214
[11] BERGMARK, A., ALZATI, L.: Fatigue Frac.of Engng. Mater. Struct., vol. 28, 2005, p. 229
[12] GOMES, MA., WRONSKI, AS., WRIGHT, CS.: Int. J. of Fracture, vol. 83, 1997, p. 207
[13] WU, MW., HWANG, KS., HUANG, HS.: Met. And Mat. Trans. A, vol. 38A, 2007, p. 1598
[14] PETROVA, V., TAMUZS, V., ROMALIS, N.: Appl. Mech. Rev., vol. 53, 2000*,* p. 117
[15] KACHANOV, M.: Int. J. Fract., vol. 120**,** 2003, p. 537
[16] LINDBORG, U.: Acta Metall ., vol. 17, 1969, p. 521
[17] CARPINTERI, A., YANG, GP.: Fatigue Frac. Engng. Mater. Struct., vol. 20, 1997, p. 1105
[18] ZATTIERI, PD., ESPINOSA, HD.: Acta Mater., vol. 49, 2001, p. 4291
[19] LI, T., YANG, W.: Fatigue, Fract. Engng. Mater. Struct*.,* vol. 25, 2002, p. 499
[20] FEDELICH, B.: Int. J. Fract., vol. 91, 1998, p. 23
[21] MA, L., WANG, X., FENG, X., YU, S.: Eng. Fracture Mech., vol. 72, 2005*,* p. 1841
[22] IRWIN, GR.: J. Appl. Mech. (Trans. ASME), vol. 29, 1962, p. 651
[23] KABÁTOVÁ, M., DUDROVÁ, E., WRONSKI, AS.: Powder Met., vol. 49, 2006, p. 363
[24] KABÁTOVÁ, M., DUDROVA, E., WRONSKI, AS.: Fatigue Frac. Engng. Mater Struct., vol. 32, 2009, p. 214
[25] KABÁTOVÁ, M., DUDROVÁ, E., WRONSKI, AS., MITCHELL, SC.: Powder Met. Progr., vol. 11, 2011, p. 104
[26] PANG, HT., REED, PAS.: Int. J. of Fatigue, vol. 25, 2003, p. 1089